J. Electrochem. Sci. Eng. **12(3)** (2022) 439-449; http://dx.doi.org/10.5599/jese.1207

Open Access : : ISSN 1847-9286

www.jESE-online.org

Original scientific paper

Facile one-pot synthesis of CuO nanospheres: Sensitive electrochemical determination of hydrazine in water effluents

N. M. Abdul Khader Jailani[1,✉], M. Chinnasamy[2] and N. S. K. Gowthaman[1,✉]

[1]*Department of Chemistry, Hajee Karutha Rowther Howdia College, Uthamapalayam - 625533, Tamilnadu, India*

[2]*Department of Chemistry, Theni College of Arts & Science, Veerapandi - 625534, Tamilnadu, India*

Corresponding authors: ✉*jailani150677@gmail.com, Tel.: +91-9442021072;* ✉*gowthamkrishna178@gmail.com*

Received: December 8, 2021; Accepted: March 18, 2022; Published: March 28, 2022

Abstract

Hydrazine (HZ) is massively used in several industrial applications. Adsorption of HZ through human skin creates carcinogenicity by disturbing the human organ system and thus, the quantification of HZ levels in environmental water samples is highly needed. The present work describes the short-term development of copper oxide nanospheres (CuO NS) by one-step wet chemical approach and their implementation on glassy carbon electrode (GCE) for the sensitive and selective quantification of the environmentally hazardous HZ. The CuO NS formation was identified by X-ray diffraction (XRD), field-emission scanning electron microscopy (FE-SEM), transmission electron microscopy (TEM) and UV-visible spectroscopy. SEM images exhibited the uniform CuO NS with an average size of 85 nm. The linker-free CuO NS modified GCE offered high electrocatalytic activity against HZ determination by showing the linear range determination in the range of 0.5 to 500 µM, with the detection limit of 63 nM (S/N=3), and sensitivity of 894.28 µA mM^{-1} cm^{-2}. Further, the developed HZ sensor displayed excellent repeatability and reproducibility and was successfully exploited for the determination of HZ in real environmental samples, implying that GCE/CuO-NS is a confident and low-cost electrochemical platform for HZ determination.

Keywords

CuO nanospheres; electrochemical sensor; voltammetry; environmental hazard

Introduction

Metal oxides have received a huge consideration in sensing applications because of their large surface area derived high photo-electrocatalytic activity, cost-effectiveness and outstanding stability [1,2]. Copper oxide nanomaterial (CuO), as a nonstoichiometric semiconductor possess a narrow bandgap of 1.2 to 1.6 eV. Due to the miniaturization and tuning of its morphological and nanomaterial features, extensive research has been focused by the research community in several applications of CuO nanomaterials, including solar cells [3], electrochromic devices [4], electrocatalysis [5-7], photocatalysis [8], gas sensing application [9] and supercapacitors [10]. The user-

friendly features of CuO nanomaterials such as low cost, high stability and durability, and eco-friendliness, motivated many researchers to develop CuO nanostructures by various synthetic routes, including hydrothermal synthesis, thermal oxidation and decomposition, vapor-phase synthesis, electron beam lithography and ultrasonic irradiation [11-13]. However, a prolonged synthetic procedure and the usage of surfactants and toxic chemicals confine the utility of CuO nanostructures in real-time applications. To overcome the aforementioned hurdles on CuO nanomaterials, this study reveals the one-step short-term surfactant-free synthetic approach for the preparation of homogenous CuO nanospheres (CuO NS) *via* wet chemical synthesis. The as-synthesized CuO NS will be tested for their utility in real-time applications.

Hydrazine (N_2H_4, HZ) is a significant chemical (bio) reagent and an effective reducing agent. It is utilized in many applications like fuel cells, chemical and pharmacy industries, pesticides, corrosion inhibitors, *etc.* HZ is, however, a highly toxic, water-soluble, colorless and flammable compound that can stimulate various severe damages, including lungs, thyroid gland, liver, spleen, liver, temporary blindness, pulmonary edema, and DNA and brain damages in the human body [14-21]. Further, HZ outflows from different industries to the environmental soil, water and air make Hz highly hazardous [22]. Therefore, the quantitative determination of HZ is a highly important task.

Electroanalytical techniques showed many advantages, like easy handling, low cost, rapid response, label-free, less laborious, and high sensitivity and selectivity [14-21]. Generally, the electrochemical determination of HZ is based on its direct oxidation on the electrode surface, where the obtained oxidation current response is directly proportional to HZ concentration. The catalytic performance of HZ oxidation is highly dependent on the selection of electrode material. It has been reported that CuO facilitates the electron transfer at much lower over-potentials because of its excellent conductivity and large specific surface area [23-28]. Few researchers have already developed CuO-based electrochemical HZ sensor [29-36]. Although the already reported sensors implied the importance of CuO in HZ determination, the lack of beneficial analytical features, including sensitivity and detection limit, and expensive synthetic procedures, made them unsuitable for real-time applications.

To achieve a simple, low-cost and reliable protocol for the development of HZ electrochemical sensor, the present work describes the one-step short-term synthesis of CuO NS and its fabrication on glassy carbon electrode (GCE) surface without the aid of a linker for the sensitive determination of an environmentally hazardous pollutant HZ. The fabricated linker-free CuO NS/GCE sensor is successfully utilized for HZ determination in industrial effluent and environmental water samples.

Experimental

Preparation of CuO NS

All chemicals used in this study were of analytical grade. The details of chemicals used in this study is given in Supplementary Material (SM). Similar to the procedure employed for CuO nanoflakes preparation [6], CuO nanospheres synthesis follows dissolving 1.0 g of copper sulfate pentahydrate in 50 mL double distilled water (DDW), and subsequent addition of 10 mL of 25 % ammonium hydroxide and 0.1 g glucose with constant stirring. The above mixture was transferred into an RB flask and refluxed to 90-120 °C under vigorous stirring for 60 min. The added glucose could act as a reducing as well as shape directing agent in the formation of CuO NS. The reaction was cooled and washed thrice with DDW till the pH of the mixture reached to ~6.5 to 7.0. Then, the reaction mixture was ultra-centrifuged with 2000 rpm. Finally, the product was vacuumized at 60 °C for 24 h to obtain a yellow solid product. The as-synthesized CuO NS was characterized by different

spectroscopic and microscopic studies and the detailed instrumentation is described in SM. Figure 1 illustrates the CuO NS formation, while the corresponding chemical reactions are as follows:

$$CuSO_4\,(aq) + NH_4OH\,(aq) \rightarrow Cu(OH)_2\,(s) + (NH_4)_2SO_4\,(aq) \quad (1)$$

$$Cu(OH)_2\,(s) \rightarrow CuO\,(s) + H_2O \quad (2)$$

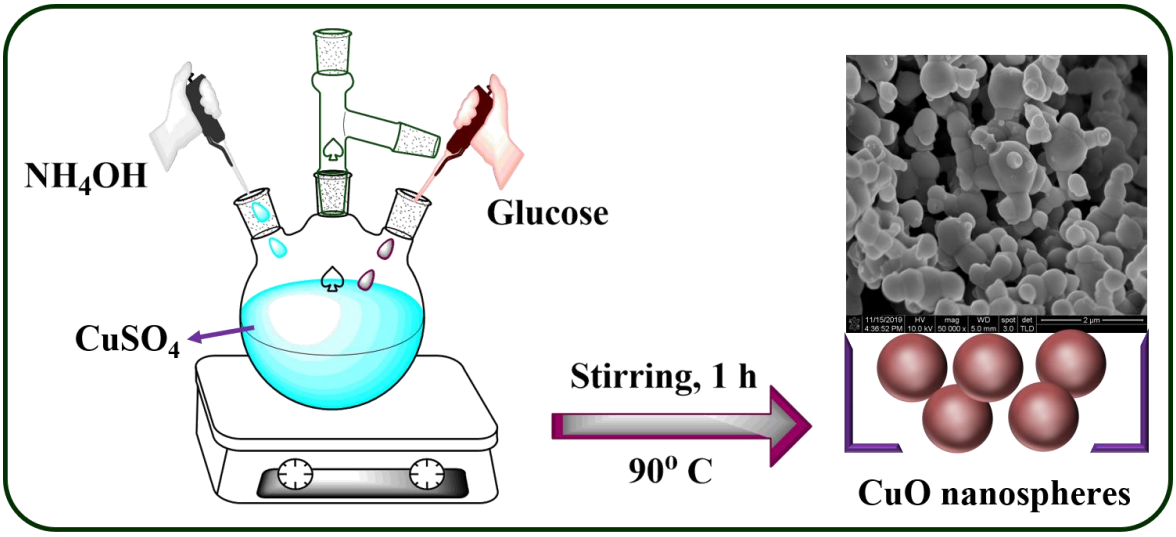

Figure 1. *Schematic representation of CuO NS preparation*

Fabrication of CuO NS on GCE

Prior to prepare the sensor electrode, GCE (geometrical area = 0.07 cm^2) was polished with 0.5 µ alumina and then ultrasonically cleaned in ethanol followed by DDW for 3 min and finally dried at room temperature. The CuO NS dispersion was prepared in DDW in the ratio of 1 mg mL^{-1} and the dispersion was ultrasonicated for 15 min. Then, 10 µL of CuO NS dispersion was pipetted out, drop-casted on the surface of well-cleaned GCE, and placed in an oven at 50˚C for 15 min. The resultant sensor electrode is represented as GCE/CuO-NS and utilized for further electrochemical studies. All electrochemical studies were conducted at CHI-660E workstation under an inert atmosphere. The detailed instrumentation is described in SM.

Preparation of environmental samples

The industrial effluents and field water samples were collected from the nearby industries and fields and the collected samples were filtered to remove any solid particles present and diluted 10 times with phosphate buffer (PB) solution (0.1 M, pH 7). After the examination of environmental samples under optimized conditions using GCE/CuO-NS sensor, known concentrations of HZ were spiked into the samples, and the results obtained from the environmental samples were compared with the results of spiked samples.

Results and discussion

Characterization by XRD, FT-IR and UV-vis spectral studies

Crystallinity, purity and crystallite size of the as-synthesized CuO NS can be identified by XRD analysis. Figure 2 displays the XRD pattern of CuO NS, which shows diffraction peaks at 22.31, 29.59, 36.66, 42.29, 61.67 and 73.50°, attributed to (100), (200), (211), (201), (123) and (402) monoclinic planes of CuO (JCPDS No. 27-0150) [26]. All diffraction peaks of CuO belong to a single phase of the monoclinic crystal system. No other peaks observed for either $Cu(OH)_2$, or the precursor, indicate

the formation of the pure monoclinic CuO NS. Scherer's formula is employed to find the crystallite size of the CuO NS by using the full-width half-maximum of (211) plane [37]:

$$X_s = k\lambda / \beta\cos\theta \quad (3)$$

where X_s denotes the crystallite size, k represents Scherer's constant, λ is wavelength, β is full-width half maximum of (211) plane and θ denotes the diffraction angle. The average crystallite size of CuO NS is found to be 37.24 nm.

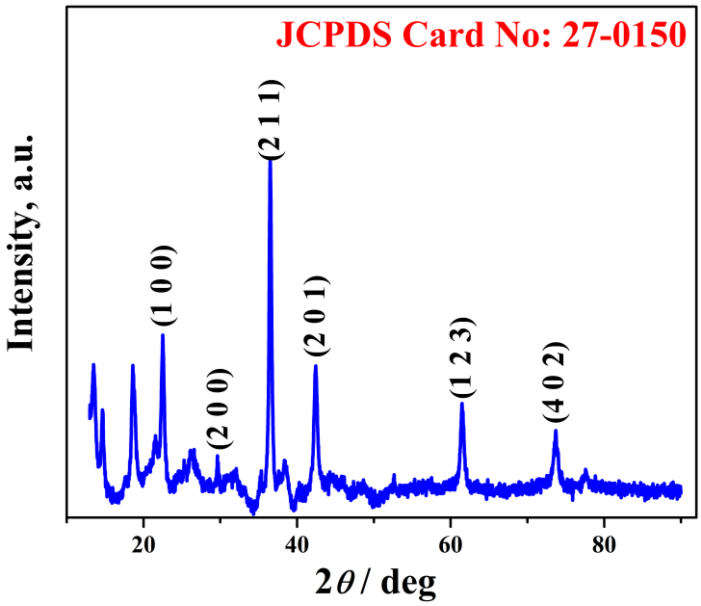

Figure 2. *XRD patterns of CuO-NS*

FT-IR spectroscopy is useful to identify reaction progress by monitoring functional groups of the molecules involved and is utilized in this work to investigate the formation of CuO NS. The recorded FT-IR spectrum for CuO NS is given in Figure S1. It shows four pronounced peaks around 700, 1378, 1620 and 3410 cm^{-1}. The low intense peak at 700 cm^{-1}, and the broad peak at 3410 cm^{-1} are respectively attributed to CuO metal-oxide vibration and hydroxyl groups, whereas the broad peak at 1620 cm^{-1} and a weak band at 1378 cm^{-1} are accredited to the O-H stretching and bending and C-H vibration peaks, respectively. The less intense peak around 1100 cm^{-1} corresponds to the vibration of C-O coordinating with metal anions.

Further, the as-prepared CuO-NS was examined by UV-vis absorption spectroscopy to study its optical behavior. The CuO-NS displayed the absorption maximum at 285 nm (Figure S-2A), which is correlated with the n-π* transition. The energy bandgap of the CuO NS was acquired from the UV-vis studies by deriving the Tauc plot (Figure S2b) [38]. The optimal energy bandgap was estimated by eq. (4),

$$\alpha_o h\nu = A\,(h\nu - E_g)^{1/2} \quad (4)$$

where, α_o stands for absorption coefficient, h denotes Plank's constant, ν represents photon frequency, A denotes proportionality constant and E_g is the energy bandgap. The plot of $(\alpha_o h\nu)^2$ *versus* hν gives the bandgap energy of CuO-NS and it was found to be 2.15 eV (Figure S-2b), indicating the direct bandgap semiconductor.

Morphological features of CuO-NS

The surface features of the synthesized CuO-NS were characterized by microscopic tools such as transmission electron microscopy (TEM) and field-emission scanning electron microscopy (FE-SEM)

attached with an energy dispersive X-ray (EDX) detector. Granules of well dispersed homogeneous spherical CuO NS were clearly observed from the TEM and FE-SEM images (Figure 3A and B) and the TEM exhibited the average size of 35 nm for the CuO NS (Figure 3A). The FE-SEM image exhibited the homogeneous and highly dense growth of CuO NS with the typical thickness of 82.7 ± 0.3 nm (Figure 3B). On the other hand, the EDX analysis of CuO NS was carried out in the range of 0 – 10 keV energy region and the recorded EDX point analysis profile is given in Figure S3. The EDX profile of CuO NS displayed the peaks for Cu (0.90, 8.04 and 8.90 eV) and oxygen (0.51 eV) elements, confirming the presence of Cu and O only in their stoichiometry.

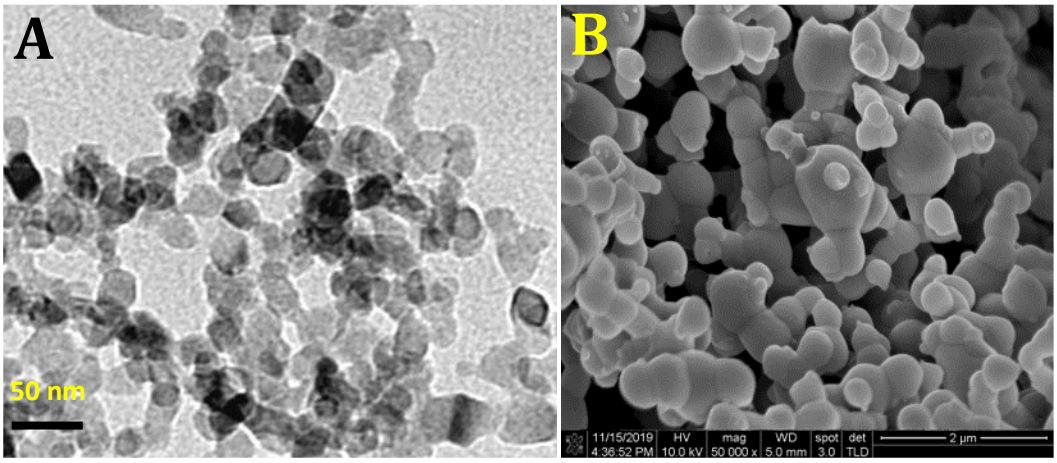

***Figure 3**. (A) TEM and (B) FE-SEM images of CuO-NS*

Characterization by electrochemical impedance spectroscopy (EIS)

Changes in the electrode-electrolyte interface and kinetics of the electrode are mainly monitored by electrochemical impedance spectroscopy (EIS). The kinetics of GCE/CuO-NS electrode was analyzed by EIS and the results are displayed in Figure S4. The electron transfer probe, 5mM $[Fe(CN)_6^{3-/4-}]$ in 0.1 M KCl, was used to analyze the reaction kinetics at GCE/CuO-NS (Figure S4). The Randles equivalent circuit (R_s[CPE-R_{ct}-W]) shown in the inset of Figure S4, was fitted to the measured EIS results. In the Randles circuit, R_s denotes solution resistance in a series connection with R_{ct} representing charge transfer resistance, and W standing for Warburg diffusion impedance, which are both in parallel with a constant phase element (CPE) accounting for double-layer impedance. The charge transfer at the electrode-electrolyte interface is revealed by the diameter of the semicircle part of the Nyquist plot. Figure S4 displays the Nyquist plots of bare GCE and GCE/CuO-NS. The bare GCE exhibited R_{ct} of 672 Ω, whereas GCE/CuO-NS displayed R_{ct} of 124 Ω. About 5-fold lower resistivity delivered by GCE/CuO-NS is mainly because of highly conductive CuO NS with homogenous morphology, which further facilitates electron transfer resulting in lower charge transfer resistance to the fabricated electrode. The above results suggested that the highly conductive CuO-NS on GCE removes the resistance barrier at the electrode-electrolyte interface. Further, the electrochemically active surface area (EASA) of different CuO-NS fabricated electrode was calculated using the Anson equation [37,39]. The EASA of CuO-NS fabricated electrode was determined as 0.37 cm^2.

Electrochemical response of CuO-NS fabricated sensor towards HZ

The electrochemical response of the CuO-NS fabricated sensor towards HZ was analyzed by cyclic voltammetry (CV) in PB solution (0.1M, pH 7.0) in the potential window of -0.2 – 1.4 V at the scan rate of 50 mV/s and the results are displayed in Figure 4A. In the absence of HZ, neither bare GCE

nor GCE/CuO-NS (dotted line) showed any faradaic current in the given potential window, indicating the electrochemical inactivity of both electrodes. After adding of 1 mM HZ into the PB solution, the bare GCE (curve a) did not exhibit any significant response by showing any oxidation current for HZ oxidation, indicating that the bare electrode is not a good catalyst for the oxidation of HZ. When the CV of GCE/CuO-NS was conducted in the presence of 1 mM HZ (curve b), it exhibited a well-shaped oxidation with the peak potential of +0.96 V. It seems that the CuO-NS with higher conductivity and EASA increased the catalytic activity by enhancing the HZ oxidation current. Although the HZ oxidation mechanism depends highly on the nature of electrode and electrolyte, the following HZ oxidation mechanism was proposed as reported early [40]:

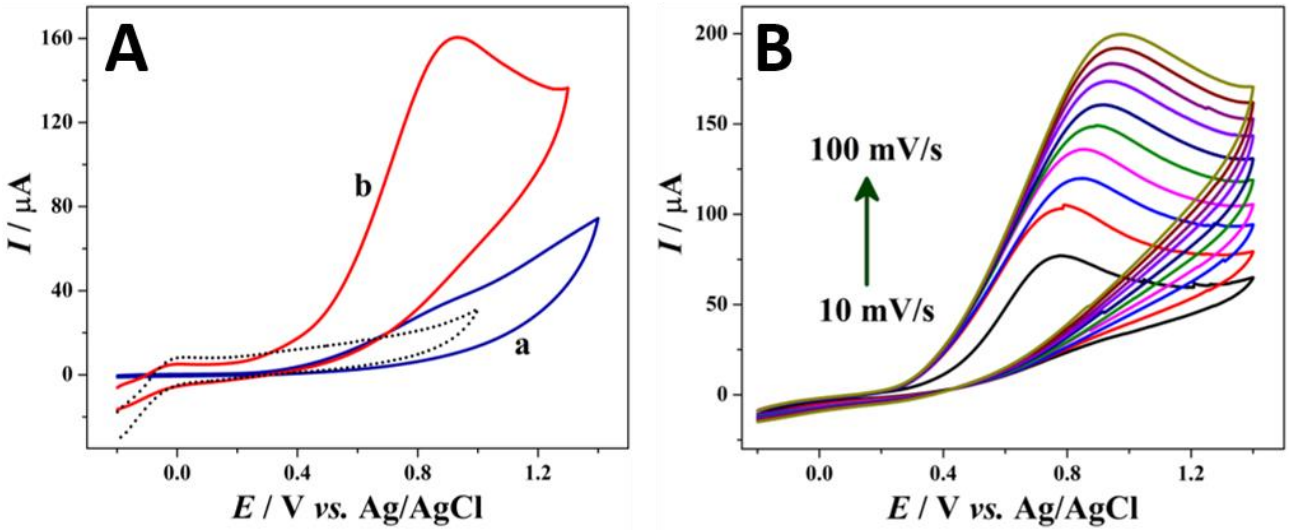

Figure 4. *CVs obtained for: (A) 1 mM HZ at (a) bare GC and (b) GC/CuO-NS electrodes at 50 mV s^{-1} in 0.1 M PB solution (pH 7); (dotted line) in absence of HZ at GC/CuO-NS electrode; (B) CVs of 1 mM HZ at GC/CuO-NS electrode at different scan rates from 10–100 mV s^{-1}*

$$N_2H_4 + H_2O \leftrightarrow N_2H_3 + H_3O^+ + e^- \text{ (slow)} \quad (5)$$

$$N_2H_3 + 3H_2O \leftrightarrow N_2 + 3H_3O^+ + 3e^- \text{ (fast)} \quad (6)$$

The rate-determining step is the slow step that proceeds by one-electron transfer (eq. 5), followed by three-electron transfer yielding N_2 final product (eq. 6). Therefore, the overall HZ oxidation reaction leads to N_2 and water formation as eco-friendly products, according to:

$$N_2H_4 + 4H_2O \leftrightarrow N_2 + 4H_3O^+ + 4e^- \quad (7)$$

The electro-oxidation of HZ at GCE/CuO-NS is illustrated in Figure 5. The interaction of CuO with HZ can be proposed as follows:

$$N_2H_4 + 2OH^- \leftrightarrow [HO\text{-}N_2H_4\text{-}OH]^{2-} \quad (8)$$

$$[HO\text{-}N_2H_4\text{-}OH]^{2-} + 4CuO \leftrightarrow 2Cu_2O + 2H_2O + 2OH^- + N_2 \quad (9)$$

$$2Cu_2O + 4OH^- \leftrightarrow 4CuO + 2H2O + 4e^- \quad (10)$$

The fabricated CuO-NS provides favorable surface conditions through unique morphological features which facilitate electron transfer at the electrode-electrolyte interface region. The excellent electronic conductivity of CuO NS coupled with high surface area enables the reaction of HZ analyte faster, along with the provision of continuous electron transport pathways. Consequently, an intensive signal for the analyte is generated, making GCE/CuO-NS be highly sensitive electrochemical HZ sensor.

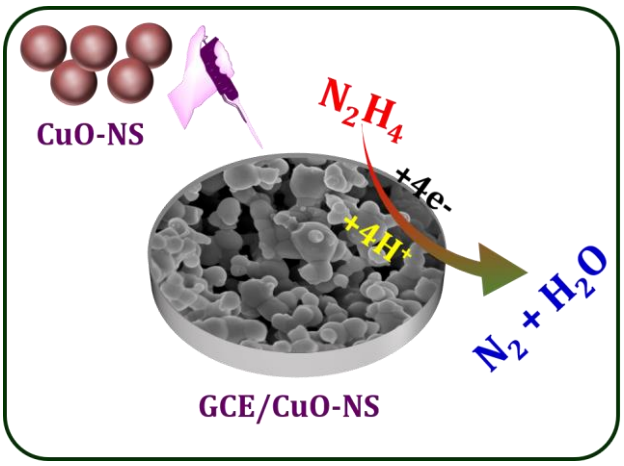

Figure 5. *Electrochemical oxidation mechanism of HZ at GCE/CuO-NS*

Figure 4B shows CVs of 1 mM of HZ at GCE/CuO-NS in PB solution (0.1 M, pH 7) at various scan rates of 10 to 100 mV s^{-1}. While increasing the scan rate with the step of 10 mV s^{-1}, the oxidation peak current of HZ was also increased with a slight shift in the oxidation potential. The plot of oxidation current *vs.* square root of scan rate is linear with the regression coefficient $R^2 = 0.9993$ (Figure S-5). The obtained straight line and R^2 value from the oxidation peak current *vs.* square root of scan rate plot suggested that the oxidation of HZ is fast, *i.e.,* a diffusion-controlled process.

Sensitive and selective determination of HZ

The sensitive determination of HZ at CuO-NS fabricated electrode is conducted by differential pulse voltammetry (DPV) technique. Figure 6A shows DPVs obtained for HZ at GCE/CuO-NS in PB solution (0.1 M, pH 7). The HZ oxidation peak was observed at 0.7 V due to the initial addition of 10 µM HZ. While increasing the concentration of HZ from 0.5 to 500 µM, the oxidation peak current was increased linearly without shifting its oxidation potential.

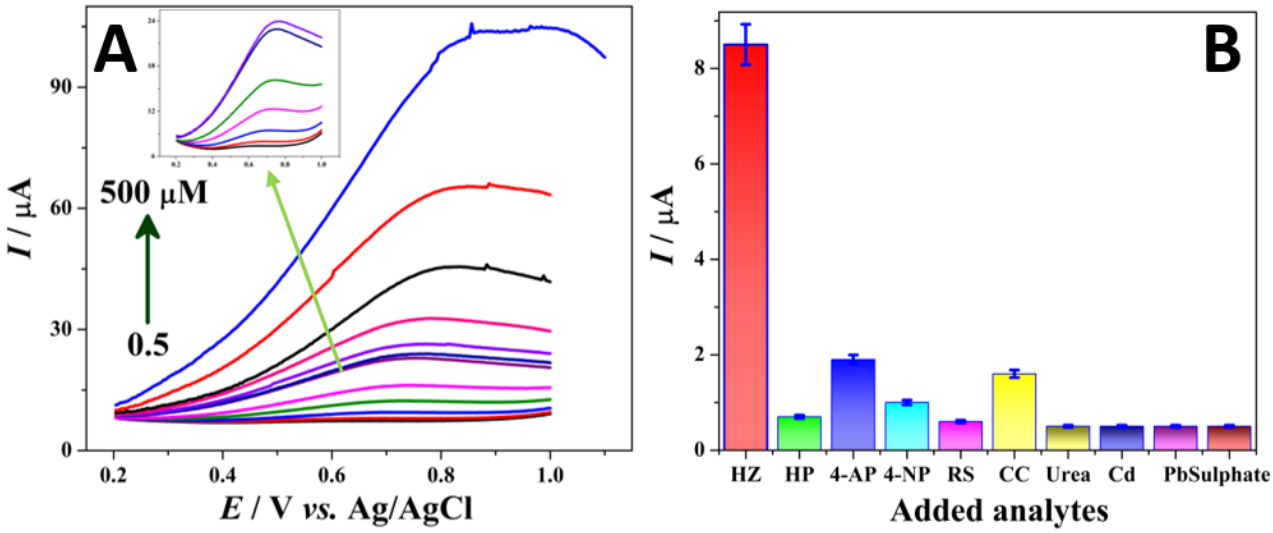

Figure 6*. (A) DPV responses of different concentrations of HZ (0.5–500 µM) and (B) anti-interference activity of HZ at GCE/CuO-NS in 0.1 M PB (pH 7.0) solution*

The plot of oxidation peak current *vs*. HZ concentration is linear with the regression equation defined as: $I_{pa} = 0.062C + 0.2207$ and $R^2 = 0.9636$ (Figure S6). The obtained linear current response suggested that the CuO NS modified electrode exhibits excellent sensitivity against HZ. The GCE/CuO-NS sensor exhibited high sensitivity of 894.28 µA mM^{-1} cm^{-2} with the limit of detection

(LOD) of 63 nM (*S*/*N* = 3) in the 0.5–500 µM wide range of HZ concentrations. The obtained sensitivity, LOD value, and wide range of HZ concentrations of linear response of CuO-NS fabricated sensor are generally superior for HZ determination compared to some recently reported sensors (Table 1) [29-36,41].

Table 1. *Comparison of GCE/CuO-NS properties for HZ determination with various CuO-based sensors*

Electrocatalyst	Medium	Linear range, µM	Detection limit, µM	Sensitivity, µA mM^{-1} cm^{-2}	Ref.
CuO-NRs[a]/GCE[b]/nafion	NaOH	0.1 – 1.0	0.01	3087	[29]
CuO NPs[c]/IL[d]/CPE[e]	pH 9.0	0.05 – 150	0.03	1.474	[30]
CuO/OMC[f]–GCE	NaOH	1-2.11×10^3	0.89	--	[31]
CuO/CNTs[g]-rGO[g]/GCE	pH 7.4	1.2 – 430	0.20	4.28	[32]
CuO/Si-P-NWs[h]/GCE	pH 7.4	1 – 5000	0.25	0.218	[33]
rGO/CuO	NaOH	0.1 – 400	9.8 ´ 10^{-3}	3.87	[34]
CuO-NPs/CPE	NaOH	100 – 800	--	19.6	[35]
Cu/Cu_2O@carbon	pH 7.4	0.25 – 800	0.022	2.37	[36]
AuNPs-rGO@NF[i]	pH 7.4	0.2 – 200	56 ´ 10^{-3}	14.635	[41]
CuO-NS/GCE	pH 7.0	0.5 – 500	63 ´ 10^{-3}	894.28	this work

[a]Nanorods; [b]glassy carbon electrode; [c]nanoparticles; [d]ionic liquid; [e]carbon paste electrode; [e]ordered mesoporous carbon; [f]carbon nanotubes; [g]reduced graphene oxide; [h]nanowires; [i]nickel foam; [j]nanospheres

The specificity of GCE/CuO-NS towards HZ detection in the presence of possible interfering molecules and ions is examined by DPV analysis. The GCE/CuO-NS showed well-defined oxidation peaks for each 10 µM HZ addition in the DPV measurement. On the other hand, no significant increase of oxidation current was observed in the presence of 50-fold higher concentrated co-interfering agents. Hydrogen peroxide (HP), 4-aminophenol (4-AP), 4-nitrophenol (4-NP), resorcinol (RS), catechol (CC) and urea, metal ions of cadmium (Cd) and lead (Pb) and common ions of sulphate (SO_4^{2-}) were tested. The corresponding response current chart is displayed in Figure 6B. The obtained results suggested that the fabricated GCE/CuO-NS sensor possesses excellent specificity towards HZ determination.

The reproducibility and repeatability of the developed HZ sensor was evaluated using three separately fabricated GCE/CuO-NS by CVs with 50 µM HZ in PB solution (0.1 M, pH 7) at a scan rate of 50 mV s^{-1}. The CV responses of three different electrodes exhibited the oxidation of HZ with 1.3 % relative standard deviation (RSD) oxidation current. Also, three consecutive CV measurements were carried out using three different electrodes and the CVs exhibited concurrent oxidation current response for HZ oxidation with an RSD of 1.5 %. Further, the GCE/CuO-NS was placed in PB solution (0.1 M, pH 7) after the CV measurements at room temperature. The CV response of the above-stored GCE/CuO-NS was analyzed for the duration of two weeks. The HZ oxidation current was decreased by about 1.4 ± 0.05 % in a week and 3.7 ± 0.05 % in two weeks compared to the initial current response. The obtained results are trustworthy for the excellent repeatability, reproducibility, and storage stability of the developed GCE/CuO-NS-based HZ sensor.

Real-time application of GCE/CuO-NS

The practical utility of the fabricated GCE/CuO-NS based HZ sensor was examined in real samples such as environmental field water and industrial effluents. These samples were obtained from field water and nearest industries. The procedure for the preparation and pre-treatment of the collected samples is given in section 2.3. DPV measurements were employed to analyze the collected environmental samples using GCE/CuO-NS. The DPVs of the collected samples did not show any oxidation response in the potential window of +0.2 to 1.0 V, indicating that samples are free from

HZ. At the same time, the HZ spiked samples exhibited a well-defined oxidation peak for HZ oxidation and the obtained oxidation currents are compared with the standard one. The GCE/CuO-NS offered 98-99 % recovery for HZ determination in real sample analysis and the obtained analytical are tabulated (Table 2). It is clear from the results listed in Table 2 that GCE/CuO-NS could deliver results that are sufficient for the environmental diagnosis of HZ. Consequently, being environmentally benign and economically viable, the proposed sensor could make a part of a robust platform for environmental pollutants determination.

Table 2. *Application of GCE/CuO NS for HZ determination in environmental samples*

Sample	HZ added, µM	HZ found, µM[a]	Recovery, %[a]
Field water	0.0	0.00	-
	5.0	5.02 ± 0.09	100.40 ± 1.81
	10.0	9.48 ± 0.19	94.80 ± 1.93
	50.0	46.51 ± 1.15	93.02 ± 2.30
Industrial effluent	0.0	0.00	-
	2.5	2.47 ± 0.06	98.80 ± 2.40
	10.0	9.91 ± 0.15	99.10 ± 1.53
	30.0	28.41 ± 0.11	94.70 ± 1.12
	100.0	93.16 ± 0.37	93.16 ± 0.37

[a]relative standard deviation

In the end, the reliability of the present sensor was validated with the high-performance liquid chromatography (HPLC) method. The results of HZ determination in real samples obtained from the present method using GCE/CuO-NS were found to be in close agreement with the results obtained *via* HPLC. The obtained agreement suggests good practicability of the developed sensor for HZ monitoring in real-time applications.

Conclusion

In this study, a facile short-term one-step method was developed for CuO nanospheres (CuO NS) synthesis, which were then fabricated on GCE without using any linker, forming CuO NS/GCE sensor for determination of the environmentally hazardous hydrazine (HZ). Cyclic and linear sweep voltammetry techniques were assessed for electrode characterization and quantification of HZ in this study. The developed GCE/CuO-NS sensor exhibited excellent specificity, repeatability, reproducibility, stability, and reliability. The GCE/CuO-NS showed the wide linear response range of HZ concentrations in the range from 0.5 to 500 µM, and the LOD was found to be 63 nM (S/N = 3), with the sensitivity towards HZ of 894.28 µA mM^{-1} cm^{-2}. The obtained results suggest that the fabricated GCE/CuO-NS could be an excellent catalyst for electrochemical sensing of environmental pollutants.

Acknowledgment: *Management of Hajee Karutha Rowther Howdia College, Uthamapalayam is gratefully acknowledged. The authors also declare that they have no conflict of interest.*

References

[1] G. Maduraiveeran, M. Sasidharan, W. Jin, *Progress in Materials Science* **106** (2019) 100574. https://doi.org/10.1016/j.pmatsci.2019.100574

[2] Y. Jia, X. Yi, Z. Li, L. Zhang, B. Yu, J. Zhang, X. Wang, X. Jia, *Talanta* **219** (2020) 121308. https://doi.org/10.1016/j.talanta.2020.121308

[3] C-H. Tsai, P-H. Fei, C-M. Lin, S-L. Shiu, *Coatings* **8** (2018) 21. https://doi.org/10.3390/coatings8010021

[4] T. J. Richardson, J. L. Slack, M. D. Rubin, *Electrochimica Acta* **46** (2001) 2281-2284. https://doi.org/10.1016/S0013-4686(01)00397-8
[5] N. S. K. Gowthaman, S. A. John, *CrystEngComm* **18** (2016) 8696−8708. https://doi.org/10.1039/C6CE01846G
[6] K. Y. Hwa, P. Karuppaiah, N. S. K. Gowthaman, V. Balakumar, S. Shankar, H. N. Lim, *Ultrasonics Sonochemistry* **58** (2019) 104649. https://doi.org/10.1016/j.ultsonch.2019.104649
[7] M. M. Alam, M. M. Rahman, A. M. Asiri, M. A. Fazal, *Journal of Materials Science: Materials in Electronics* **32** (2021) 5259–5273. https://doi.org/10.1007/s10854-021-05257-2
[8] K. Sekar, C. Chuaicham, B. Vellaichamy, W. Li, W. Zhuang, X. Lu, B. Ohtani, K. Sasaki, *Applied Catalysis B: Environmental* **294** (2021) 120221. https://doi.org/10.1016/j.apcatb.2021.120221
[9] S. Steinhauer, E. Brunet, T. Maier, G.C. Mutinati, A. Köck, O. Freudenberg, C. Gspan, W. Grogger, A. Neuhold, R. Resel, *Sensors and Actuators B: Chemical* **187** (2013) 50-57. https://doi.org/10.1016/j.snb.2012.09.034
[10] S. K. Shinde, H. M. Yadav, G. S. Ghodake, A. A. Kadam, V. S. Kumbhar, J. Yang, K. Hwang, A. D. Jagadale, S. Kumar, D. Y. Kim, *Colloids and Surfaces B: Biointerfaces* **181** (2019) 1004-1011. https://doi.org/10.1016/j.colsurfb.2019.05.079
[11] A. N. S. Rao, V. T. Venkatarangaiah, *Journal of Electrochemical Science and Engineering* **4** (2014) 97-110. https://doi.org/10.5599/jese.2014.0063
[12] M. F. Shabik, M. M. Hasan, K. A. Alamry, M. M. Rahman, Y. Nagao, M. A. Hasnat, *Journal of Electroanalytical Chemistry* **897** (2021) 115592. https://doi.org/10.1016/j.jelechem.2021.115592
[13] M. M. Rahman, S. B. Khan, H. M. Marwani, A. M. Asiri, K. A. Alamry, A. O. Al-Youbi, *Talanta* **104** (2013) 75-82. https://doi.org/10.1016/j.talanta.2012.11.031
[14] J. D. Lović, *Journal of Electrochemical Science and Engineering* **12(2)** (2022) 275-282. https://doi.org/10.5599/jese.1166
[15] M. M. Rahman, V. G. Alfonso, F. Fabregat-Santiago, J. Bisquert, A. M. Asiri, A. A. Alshehri, H. A. Albar, *Microchimica Acta* **184** (2017) 2123-2129. https://doi.org/10.1007/s00604-017-2228-x
[16] N. S. K. Gowthaman, S. Shankar, S. A. John, *ACS Sustainable Chemistry & Engineering* **6** (2018) 17302-–17313. https://doi.org/10.1021/acssuschemeng.8b04777
[17] M. M. Rahman, J. Ahmed, A. M. Asiri, I. A. Siddiquey, M. A. Hasnat, *RSC Advances* **6** (2016) 90470-90479. https://doi.org/10.1039/C6RA08772H
[18] H. Akhter, J. Murshed, M.A. Rashed, Y. Oshim, Y. Nagao, M. M. Rahman, A. M. Asiri, M.A. Hasnat, M. N. Uddin, I.A. Siddiquey, *Journal of Alloys and Compounds* **698** (2017) 921-929. https://doi.org/10.1016/j.jallcom.2016.12.266
[19] M. M. Rahman, M. M. Alam, A. M. Asiri, *New Journal of Chemistry* **42** (2018) 10263-10270. https://doi.org/10.1039/C8NJ01750F
[20] M. M. Alam, A. M. Asiri, M. M. Rahman, *Materials Chemistry and Physics* **243** (2020) 122658. https://doi.org/10.1016/j.matchemphys.2020.122658
[21] M. M. Rahman, B. M. Abu-Zied, A. M. Asiri, *RSC Advances* **7** (2017) 21164-21174. https://doi.org/10.1039/C7RA00952F
[22] *Environmental Health Criteria 68: Hydrazine*; World Health Organization (WHO), Geneva, Switzerland, (1987) 1−89. ISBN 92 4 154268 3
[23] M. A. Subhan, P. C. Saha, J. Ahmed, A. M. Asiri, M. Al-Mamun, M. M. Rahman, *Materials Advances* **1** (2020) 2831-2839. https://doi.org/10.1039/D0MA00629G
[24] M. M. Rahman, S. B. Khan, A. M. Asiri, H. M. Marwani, A. H. Qusti, *Composites Part B: Engineering* **54** (2013) 215-223. https://doi.org/10.1016/j.compositesb.2013.05.018

[25] M. Faisal, S. B. Khan, M. M. Rahman, A. Jamal, A. Umar, *Materials Letters* **65** (2011) 1400-1403. https://doi.org/10.1016/j.matlet.2011.02.013
[26] S. B. Khan, M. Faisal, M. M. Rahman, I. A. Abdel-Latif, A. A. Ismail, K. Akhtar, A. Al-Hajry, A. M. Asiri, K. A. Alamry, *New Journal of Chemistry* **37** (2013) 1098-1104. https://doi.org/10.1039/C3NJ40928G
[27] M. M. Hussain, A. M. Asiri, M. M. Rahman, *New Journal of Chemistry* **44** (2020) 9775-9787. https://doi.org/10.1039/D0NJ01715A
[28] A. M. Asiri, W. A. Adeosun, M. M. Rahman, *Microchemical Journal* **159** (2020) 105527. https://doi.org/10.1016/j.microc.2020.105527
[29] R. A. Soomro, Q. Baloach, A. Tahira, Z. H. Ibupoto, G. Q. Khaskheli, Sirajuddin, V. K. Deewani, K. R. Hallam, K. Rajar, M. Willander, *Microsystem Technologies* **23** (2017) 731–738. https://doi.org/10.1007/s00542-015-2726-x
[30] N. Teymoori, J. B. Raoof, M. A. Khalilzadeh, R. Ojani, *Journal of the Iranian Chemical Society* **15** (2018) 2271–2279. https://doi.org/10.1007/s13738-018-1416-x
[31] L. Wang, T. Meng, H. Jia, Y. Feng, T. Gong, H. Wang, Y. Zhang, *Journal of Colloid and Interface Science* **549** (2019) 98-104. https://doi.org/10.1016/j.jcis.2019.04.063
[32] Z. Zhao, W. Wang, W. Tang, Y. Xie, Y. Li, J. Song, S. Zhuiykov, J. Hu, W. Gong, *Ionics* **26** (2020) 2599–2609. https://doi.org/10.1007/s11581-019-03305-w
[33] Z. Guo, M.L. Seol, M. S. Kim, J. H. Ahn, Y. K. Choi, J. H. Liu, X. J. Huang, *Nanoscale* **4** (2012) 7525–7531. https://doi.org/10.1039/C2NR32556J
[34] K. Ramachandran, K. Babu, G. G. Kumar, A. R. Kim, D. J. Yoo, *Science of Advanced Materials* **7** (2015) 329-336. https://doi.org/10.1166/sam.2015.2025
[35] G. Karim-Nezhad, R. Jafarloo, P. S. Dorraji, *Electrochimica Acta* **54** (2009) 5721–5726. https://doi.org/10.1016/j.electacta.2009.05.019
[36] Z. Zhao, Y. Wang, P. Li, S. Sang, W. Zhang, J. Hu, K. Lian, *Analytical Methods* **7** (2015) 9040-9046. https://doi.org/10.1039/C5AY02122G
[37] N. S. K. Gowthaman, S. A. John, *CrystEngComm* **19** (2017) 5369-5380. https://doi.org/10.1039/C7CE01044C
[38] N. S. K. Gowthaman, H. N. Lim, V. Balakumar, S. Shankar, *Ultrasonics Sonochemistry* **61** (2020) 104828. https://doi.org/10.1016/j.ultsonch.2019.104828
[39] V. Fragkou, Y. Ge, G. Steiner, D. Freeman, N. Bartetzko, A. P. F. Turner, *International Journal of Electrochemical Science* **7** (2012) 6214-6220. http://electrochemsci.org/papers/vol7/7076214.pdf
[40] N. S. K. Gowthaman, S. A. John, *RSC Advances* **5** (2015) 42369-42375. https://doi.org/10.1039/C5RA06537B
[41] W. Wang, Z. Zhao, H. Yang, P. Li, Z. Yu, W. Zhang, J. Shi, J. Hu, Y. Chen, *Journal of Materials Science* **55** (2020) 9470-9482. https://doi.org/10.1007/s10853-020-04684-6